HHS Public Access

Author manuscript

Biochim Biophys Acta Gen Subj. Author manuscript; available in PMC 2021 August 27.

Published in final edited form as:

Biochim Biophys Acta Gen Subj. 2021 April ; 1865(4): 129798. doi:10.1016/j.bbagen.2020.129798.

J or H mtDNA haplogroups in retinal pigment epithelial cells: Effects on cell physiology, cargo in extracellular vesicles, and differential uptake of such vesicles by naïve recipient cells

Crystal Nicholson[a,1], **Masaaki Ishii**[a,1], **Balasubramaniam Annamalai**[a], **Kyrie Chandler**[a], **Marilyn Chwa**[b], **M. Cristina Kenney**[b], **Navjot Shah**[a], **Bärbel Rohrer**[a,c,d,*]

[a]Department of Ophthalmology, Medical University of South Carolina, Charleston, SC 29425, United States of America

[b]Gavin Herbert Eye Institute, Department of Ophthalmology, University of California Irvine, Irvine, CA 92697, United States of America

[c]Department of Neurosciences Medical University of South Carolina, Charleston, SC 29425, United States of America

[d]Ralph H. Johnson VA Medical Center, Charleston, SC 29401, United States of America

Abstract

Purpose: Extracellular vesicles (EVs) are predicted to represent the internal state of cells. In polarized RPE monolayers, EVs can mediate long-distance communication, requiring endocytosis via protein-protein interactions. EV uptake from oxidatively stressed donor cells triggers loss in transepithelial resistance (TER) in recipient monolayers mediated by HDAC6. Here, we examine EVs released from RPE cells with identical nuclear genes but different mitochondrial (mt)DNA haplogroups (H, J). J-cybrids produce less ATP, and the J-haplogroup is associated with a higher risk for age-related macular degeneration.

Methods: Cells were grown as mature monolayers to either collect EVs from apical surfaces or to serve as naïve recipient cells. Transfer assays, transferring EVs to a recipient monolayer were performed, monitoring TER and EV-uptake. The presence of known EV surface proteins was quantified by protein chemistry.

Results: H- and J-cybrids were confirmed to exhibit different levels of TER and energy metabolism. EVs from J-cybrids reduced TER in recipient ARPE-19 cells, whereas EVs from H-cybrids were ineffective. TER reduction was mediated by HDAC6 activity, and EV uptake required interaction between integrin and its ligands and surface proteoglycans. Protein quantifications confirmed elevated levels of fibronectin and annexin A2 on J-cybrid EVs.

Conclusions: We speculate that RPE EVs have a finite set of ligands (membrane proteoglycans and integrins and/or annexin A2) that are elevated in EVs from stressed cells; and that if EVs

*Corresponding author at: Department of Ophthalmology, Medical University of South Carolina, 167 Ashley Avenue, Charleston, SC 29425, United States of America. rohrer@musc.edu (B. Rohrer).

[1]These two authors contributed equally.

Declaration of Competing Interest

The authors have no financial or non-financial competing interests to disclose.

released by the RPE could be captured from serum, that they might provide a disease biomarker of RPE-dependent diseases.

Keywords

Retinal pigment epithelium; Extracellular vesicles; mtDNA cybrids; OXPHOS; Ligands; Age-related macular degeneration

1. Introduction

Age-related macular degeneration (AMD) is a slowly progressing multifactorial disease involving genetic abnormalities and environmental insults [1]. Inflammation, smoking [2] and polymorphisms in some complement proteins can increase the risk for AMD [3]. Hence, the concept has emerged that abnormalities in controlling oxidative stress and the complement system may lead to inflammation in retinal pigment epithelium (RPE)/Bruch's membrane, generating a pathological environment favorable for AMD development [4].

A feature of atrophic AMD is localized damage and ultimately loss of RPE cells, predominantly at the posterior pole. Mitochondria play an essential role in cell health and death. The majority of the RPE cell's energy is generated in the mitochondria by oxidative phosphorylation (OXPHOS) [5]. Mitochondria contain circular DNA, inherited through the maternal linage. The highly polymorphic mitochondrial DNA is critical for energy production, since 13/37 genes code for protein subunits used in OXPHOS. In OXPHOS, a proton gradient across the mitochondrial inner membrane is created, which is used to generate ATP. Under certain conditions however, partial uncoupling of the two processes occurs, increasing the proton leak and decreasing ATP production. Importantly, single nucleotide polymorphisms of the mitochondrial DNA (haplogroups) can change mitochondrial function [6]. These haplogroups are associated with geographic origins of different populations, allowing the establishment of a mtDNA phylogenetic tree, and providing a tool for medical genetics [7]. Interestingly, the J, T, and U haplogroups have been found to be associated with AMD [8–11], while the H-haplogroup is not [12], yet all are of European origin. While it is unclear how mtDNA variants contribute to AMD risk and by which cellular mechanisms or pathways, Kenney and coworkers have speculated that the altered energy metabolism and modified expression of nuclear genes might play a role [13]. In other diseases such as Parkinson's disease and Alzheimer's disease, mitochondrial cybrids have provided important insights as to how mtDNA induces differences in mitochondrial biology, and how altered mitochondrial function influences cell physiology; however animal-based models to assess these mtDNA genotype–phenotype correlations should be developed and studied in addition [14]. We have created cybrids (cytoplasmic hybrids) which were generated by introducing mitochondria from individuals that are either haplogroup J or H into an immortalized human RPE cell (ARPE-19 cells) from which the mitochondria (U5 haplogroup) were removed, so the two cybrids carry the same nuclear genes [13]. Specifically, while cell viability is similar between the two APRE-19 cell haplogroups, J-cybrids generate significantly less reactive oxygen species and ATP when compared to H-cybrids. In addition, expression levels for nuclear genes involved in complement and metabolism are also altered in J- versus H-cybrids [13]. We have shown

that mitochondrial ATP production is affected by age; human embryonic RPE cells have small, dynamic mitochondria that generate large amounts of ATP; cells derived from old donors have larger, less dynamic mitochondria that generate smaller amounts of ATP [15]. And age-related accumulation of damaged mtDNA has been reported in the RPE, which is also exacerbated by disease [16] and in subjects with AMD gene mutations [17].

RPE pathology in AMD has been shown to be initiated in multiple patches at the posterior pole, rather than to emanate from a single location. We have speculated that this pattern might be mediated by short-distance communication, such as gap-junction communication [18,19], and long-distance communication that might be mediated by extracellular vesicles (EVs) [20], between diseased and healthy parts of the tissue.

EVs are small vesicles with an approximate size of 40–150 nm. They are released from many different cells and consequently have been isolated from many body fluids. Our understanding of EVs has covered the spectrum from EVs as the cell's garbage bin, to intercellular communication devices, to promising therapeutic targets [21]. This change in sentiment occurred as we discovered that EVs not only contain protein, but also RNA, miRNA, lcRNA and play a crucial role in intercellular communication [22].

We have started characterizing EVs in intercellular communication in RPE monolayers. Previously, we have shown that EVs are released from both the apical and basal surfaces of ARPE-19, the same cells used here but with a U5 mitochondrial DNA haplogroup, as well as primary porcine RPE cells when grown as stable monolayers [20]. The ARPE-19 cell EVs were carefully characterized based on morphology, size and markers based on MISEC 2018 guidelines [23]. In short, nanoparticle tracking analysis confirmed that the average diameter of EVs was 127.5 ± 10.0 nm with an average zeta-potential of −25.70 ± 3.07 mV. Transmission electron microscopy (EM) demonstrated that some of the vesicles exhibited the central depression characteristic for exosomes, and immunogold labelling EM confirmed the presence of the exosome marker tetraspanin protein CD81, previously shown by Knickelbein and colleagues to be present on ARPE-19 cell EVs [24]. Additional experiments to confirm purity of the samples using ELISA measurements to quantify syntenin-1 (exosome marker) [25] and ApoB (modified lipo-protein particles known to be secreted by ARPE-19 cells) [26], revealed that the EV preparations contained syntenin-1, whereas no ApoB was detected [20]. Furthermore, two additional markers, annexin A2 and fibronectin were identified in these vesicles; two proteins that are within the list of top 100 proteins that are often identified in exosomes (exocarta.org). Follow-up experiments were performed on ARPE-19 cell EVs to characterize their potential function in cell-cell communication [20,27]. Using transfer assays, adding labeled or un-labeled EVs released from either control or H_2O_2-stimulated monolayers, we showed EV uptake by confocal microscopy and a functional readout [20]. Confocal microscopy demonstrated that EVs from oxidatively stressed cells added to a monolayer of naïve recipient cells were taken up within ~10–20 min, with very few EVs remaining on the cell surface. In contrast, EVs from control were internalized slowly (taking ~100 min) and incompletely, with ~80% of the control EVs remaining outside the cell [20]. As a functional readout, we demonstrated that stress EVs taken up by recipient cells resulted in a loss of barrier function (transepithelial resistance [TER]) that was mediated by HDAC6 activity present in the EVs [20]. TER loss

was dependent upon the presence of EVs and not other secreted proteins, as ARPE-19 cell supernatant depleted of EVs, was ineffective [20]. Using these two readouts (imaging and TER), we showed that uptake is dependent on ligands on the EV surface [27]. Those include three ligand-receptor interactions, integrins, proteoglycans, and annexin A2. Elevated levels of these ligands were identified on stress EVs when compared to control EVs; and uptake could be inhibited by interfering with integrin signaling, stripping of proteoglycans from the recipient cells as well as knocking down gene expression for annexin A2 [20,27]. In contrast, elevating annexin A2 gene expression allowed for uptake of EVs from non-stressed cells [20]. These results suggest that EVs from stressed cells differ from their control counterparts in the level of ligands present on their surfaces. Not only does that affect uptake by recipient cells, but suggests that oxidative stress in general leads to increased targeting of ligands, such as fibronectin and annexin A2, to EVs.

Here, we ask the question whether oxidative stress mediated by mitochondrial haplogroups results in the production of EVs with similar characteristics as those generated by H_2O_2.

2. Material and methods

2.1. Cell culture

Parent ARPE-19 cells (ATCC® CRL-2302™; American Type Culture Collection, Manassas VA, obtained as passage 20) that carry the U5 mitochondrial DNA haplogroup between passages 20–35 and ARPE-19 cell lines that carry either the H- or J-haplogroup (called transmitochondrial cybrids) [28] between passages 10–18 were expanded in 100 mm dishes (Thermo Fisher) with Dulbecco's modified Eagle's medium (DMEM). ARPE-19 cells were provided with 10% fetal bovine serum (FBS), cybrids with 10% dialyzed fetal bovine serum (dFBS), and 1× antibiotic-antimycotic for 7 days or until 100% confluent. Once confluent, cells were washed with 1× Phosphate-buffered saline (PBS, Gibco), trypsinized with 0.05% trypsin (Gibco), seeded at 3.0×10^5 cells on 6-well transwell filters (Costar), and grown for 4 weeks, or on 96-well custom plates designed for use in the Seahorse assay. Passages 20–35 were used for ARPE-19 cells to match them for comparison with our previous manuscript [27].

2.2. Monolayer development and transepithelial resistance assay

Upon reaching confluency on transwell plates, tight junction formation and creating of a polarized monolayer was enabled by step-wise FBS or dialyzed FBS (dFBS) reduction to 1%. During the first week, cells were grown in the presence of 10% FBS or dFBS in the top and 2% on the bottom of transwells (10%/2% top/bottom), followed by a weekly step-wise reduction of FBS or dFBS from 10%/2% to 2%/2% to 1%/1% top/bottom. Finally, FBS or dFBS was removed completely for the final 2–3 media changes prior to the experiments to remove any serum-derived EVs.

Monolayer integrity was assessed by TER measurements using an EVOM volt-ohmmeter (World Precision Instruments) as described [29], with monolayers considered stable when TER was repeatedly measured as ~40–45 Ω cm^2 [30].

2.3. Seahorse assay

Oxygen consumption rate (OCR) and extracellular acidification rate (ECAR) measurements of cybrids were performed using a Seahorse Bioscience XF96 instrument (Seahorse Bioscience, Billerica, MD), as previously published [31]. Cells were plated at a density of 1.4×10^4 cells on 96-well custom plates designed for use in the XF96 and grown to ~90% confluency in DMEM +10% dFBS (or FBS), after which the dFBS (or FBS) was reduced to 1% for 24 h and completely eliminated for the last 48 h. No cells were plated in outer wells, 100 μL media was added for warmth/humidity. Prior to running the experiment, the growth medium was removed and the cells were washed with PBS containing Ca^{2+}/Mg^{2+} (pH 7.4), which was then aspirated and replaced with 150 μL reduced serum (RS) buffer containing 1.8 mM $CaCl_2$, 0.6 mM $MgCl_2$, 0.5 mM KH_2PO_4, 6.3 mM KCl, 0.5 mM Na_2HPO_4, 135 mM NaCl, 5.6 mM glucose, 1 mM glutamine, minimum essential medium (MEM) amino acids solution, MEM non-essential amino acids, MEM vitamin solution, penicillin/streptomycin, 1% bovine serum albumin (BSA, factor V fatty-acid-free), 1% FBS, and insulin (100 nM); the pH was adjusted to 7.4 prior to filter sterilization. The XF-96 protocol consists of three measurements each (1 measurement/5 min) of basal OCR/ECAR, and after injections of oligomycin (1.0 μM), *p*-trifluoromethoxyphenylhydrazone (FCCP) (1.0 μM), and rotenone and antimycin A (each at 2 μM) optimized for ARPE-19 cells (data not shown). Oxygen consumption rates were calculated from the continuous average slope of the O_2 partitioning among plastic, atmosphere, and cellular uptake; and pH levels were calculated, which represent lactic acid extrusion [31]. Data were normalized to area of well covered by cells using the IncuCyte Zoom system imaging in high definition phase-contrast mode (Essen BioScience, Ann Arbor, MI). The following parameters are reported for OCR: basal respiration, ATP production, maximum respiration, proton leak, spare respiratory capacity and coupling efficiency, using the Agilent Seahorse XF Cell Mito Stress Test Report Generator; for ECAR, we only report ECAR after eliminating ATP synthase with oligomycin. Results are presented as mean ± SEM. The average of 28/29 wells for each condition is reported.

2.4. EV generation and concentration

To trigger EV release from oxidatively stressed ARPE-19 cells grown on 6 well transwell plates (~1×10^6 cells per well), monolayers switched to serum-free media, were stimulated apically with 0.5 mM H_2O_2 (Sigma Aldrich) as described [20]. Supernatants from ARPE-19 cells or cybrids were collected from the apical side only (2 mL per well, pooled samples from 6 wells for a total of 10 mL). After preclearing the samples using a low speed spin (3000 *g*), EV isolation was performed using Exoquick-TC (Systems Biosciences) according to the manufacturer's instructions. Exoquick-TC (10%) was added to the 10 mL of culture media, incubated overnight at 4 °C, followed by pelleting of the EVs by centrifugation at 1600 *g* for 35 min and resuspension into fresh media. The ZetaView PMX 110 (Particle Metrix, Meerbusch, Germany) and its corresponding software (ZetaView 8.02.28) was used to obtain EV concentration and size, as described previously in detail [20,27]. Protein concentration in the samples was assessed using the PierceTM BCA Protein Assay kit (Thermo Fisher Scientific, Waltham, MA, USA; 23225) according to the manufacturer's instructions. We have submitted all relevant data of our experiments to the EV-TRACK knowledge-base (EV-TRACK ID: EV200087) [32].

2.5. Transfer assays

Cell-cell or more precisely, EV-cell communication was studied using transfer assays as described previously [20,27]. Purified apically released H-EVs, J-EVs or ARPE-19 cell EVs (control or H_2O_2) were resuspended in fresh serum-free media and transferred to the apical compartment of naïve recipient monolayers of the same age and TER as donor cells. To keep these experiments physiologically relevant, EVs corresponding to the average amount of EVs released from cells from a single well were transferred per experimental condition. TER measurements were performed prior to the transfer (designated as 0 h) and after incubation of 4 h for each treatment with 3 measurements taken from different points on the transwell. Each TER experiment reflects the average of 3 independent experiments with 3 biological replicates of transwells, unless otherwise indicated.

Some recipient monolayers were pre-treated for 30–60 min with compounds known to inhibit EV uptake [27] or block histone deacetylase 6 (HDAC6) activity [20], including filipin (blocks lipid-based interactions, 250 μg/mL, Sigma Aldrich), arginylglycylaspartic acid (RGD) peptide (blocks integrin signaling, 10 μg/mL, Sigma Aldrich), heparinase (to remove surface proteoglycans, 10 μg/mL, Sigma Aldrich) and the class I and II mammalian HDAC family inhibitor trichostatin A (TSA, 100 nM, Sigma).

2.6. Protein analysis

Ligands were analyzed by Western blotting or ELISA, HDAC6 activity was assessed using a homogenous fluorescence release HDAC deacetylase assay. For each assay, samples from 3 independent experiments were analyzed. Equal number of EVs were solubilized and subjected to analysis as published previously [20,27]. In short, after samples (1.7×10^{10} EVs) were separated by electrophoresis on 4–20% Criterion™ TGX™ Precast Gels (Bio-Rad Laboratories, Inc), and proteins transferred to PVDF membranes, membranes were probed with primary antibodies against annexin-A2 (1:1000; ab41803, Abcam) or fibronectin (1:1000; 610077, BD Bioscience) followed by visualization with horseradish peroxidase-conjugated secondary antibodies and Clarity™ Western ECL Blotting Substrate (Bio-Rad Laboratories) with chemiluminescent detection, using 10 s exposure times [27]. The glypican 1 ELISA was carried out according to manufacturer instructions (ELH-GPC1–1, Ray-BioTech) using a microplate reader, analyzing 1.38×10^{11} EVs per sample as published previously [27]. HDAC activity was measured with a homogenous fluorescence release HDAC deacetylase assay, incubating EVs (1×10^9 per reaction) with (AMC)-K(*Ac*)GL-Ac substrate to assess class I HDACs (HDACs 1, 2, 3, 6 and 10) in the presence of MS-275 to block HDAC 1, 2 and 3 activities [33] and activity was calculated as reported [34].

2.7. Imaging

Cells were plated in glass bottom 96-well plates (Mattek; Ashland, MA) analyzing 3 wells per condition. For imaging, recipient cells were labeled with the cytoplasmic dye CellTrackerTM Red (1:1000; ThermoFisher, Waltham, MA) and the nuclear dye Hoechst 33342 (Thermofisher). To enable tracking of EV uptake, EVs were labeled with ExoGlow (Systems Biosciences, EXOC300A-1) according to the manufacturer's instructions, with excess label being removed by resuspending the labeled EV pellet in PBS, followed by

repurification with ExoQuick as published previously [20,27]. Live-cell imaging of EVs was performed 2 h after adding EVs (5.2×10^8) using the UltraViewVoX spinning disk confocal microscope (Eclipse Ti, Nikon, Tokyo, Japan), running Volocity software (Perkin Elmer, Wokingham, UK) as published previously [18,20]. The particle analyzer module in ImageJ was used to detect and quantify the EV (green) - CellTracker (red) colocalized particles (yellow), and the number of EVs is expressed as the ratio of internalized experimental EVs when compared to control EVs.

2.8. Statistics

Data are presented as mean ± SEM or mean ± stdev, depending on the number of samples analyzed. For biochemical and TER assays, single comparisons were analyzed using unpaired *t*-tests; experiments containing multiple parameters were analyzed using ANOVA with Bonferroni correction (Statview; SAS Institute, Cary NC). For Seahorse and imaging, data analysis was performed using Prism GraphPad software (San Diego, CA) using a Student's *t*-test.

3. Results

3.1. Transmitochondrial J-cybrids have reduced energy metabolism

Cybrids (cytoplasmic hybrids) are cells with identical nuclear genes but different mitochondrial DNA, generated by introducing mitochondria of choice into rho0 cells from which mitochondria were removed [7]. The RPE cybrids chosen here are the H- and J-haplogroups. The H-haplogroup is associated with lower, the J-haplogroup with higher risk of developing AMD [8–12]. Cybrids with the H-haplogroup have been reported to grow and proliferate slower than those with the J-haplogroup, but generate ~40% more ATP, which is paralleled by altered expression in metabolism genes [7]. Here we tested the cells ability to generate a monolayer and confirmed and expanded on the analysis of their energy metabolism.

ARPE19 cells grown as monolayers on transwell plates develop a stable TER within 10–14 days after plating [30]. As the growth rates differ between the two haplogroup, TER measurements were delayed until 6 weeks after plating. At that developmental stage, TER levels differed by ~15% between the two cell types, with barrier function being significantly lower in J- when compared to H-cybrids (J-cybrids 38.9 ± 5.57 versus H-cybrids 45.7 ± 4.86 Ωcm^2; $P < 0.001$).

Energy metabolism was analyzed using Seahorse assays. The Seahorse technology allows for the analysis of oxidative phosphorylation and glycolysis in a 96-well plate format in parallel. Specifically, the two sensors lowered towards the plated cells measure oxygen consumption rate (oxygen tension; OCR) (Fig. 1A) and lactic acid production rate (pH, extracellular acidification rate; ECAR) (Fig. 1B) in the media. Aspects of energy metabolism can be evaluated using chemicals that interfere at different stages of the electron transport chain. OCR and ECAR were measured simultaneously, and evaluated at baseline, after ATP synthase inhibition (complex V; oligomycin), after the addition of FCCP to collapse the proton gradient, and after complex III and complex I inhibition (rotenone and

antimycin A) (Fig. 1C, D). At baseline, OCR levels were reduced in J- when compared to H-cybrids by ~20%, as were ECAR levels. Additional analyses on OCR reveal that H- and J-cybrids differ from each other in ATP synthase activity, proton leak, maximum respiration and coupling efficiency, with H-cells producing more ATP, having a reduced proton leak and a more tightly coupled electron transport chain (ETC). Taken together, H-cybrids generate significantly more ATP than J-cybrids represented by elevated OXPHOS parameters and increased glycolysis to supply substrate to the tricarboxylic acid (TCA) cycle (Fig. 1E).

3.1.1. Bystander effect elicited by J-cybrids EVs requires ligand-dependent EV uptake by naive recipient cells—ARPE-19 cells and the ARPE-19 cell J- and H-cybrids were grown as monolayers for 5–6 weeks to form polarized cells and EVs released from the apical side into serum-free media collected. We have carefully characterized the vesicles released from ARPE-19 cell in a previous publication, which we have outlined in the Introduction and have not repeated these experiments here [20]. However, based on our published data on size range, morphology, zeta-potential and exosome-specific protein enrichment (presence of CD81, annexin A2, fibronectin and lack of ApoB) [20,27], we suggest that the EVs from ARPE-19 cells isolated using ExoQuick isolation are a mixture of microvesicles and exosomes [23]. Here we confirmed that the cybrids and naive ARPE-19 release between 1.5 and 5.5 × 10^{10} EVs per mL of media cells towards the apical side over the 72 h collection period, using Nanoparticle Tracking Analysis. This corresponds to on average 1.54 ± 0.27 μg/mL of EV protein or a ratio of particles to protein [log (particle concentration/protein concentration)] [35] of 10.1 ± 0.37. Their average diameter range from 128.1 ± 5.09 nm for ARPE-19 cells, 131.7 ± 3.78 nm for H-and 138.6 ± 3.59 nm for J-cybrids, with no statistical significance between the 3 groups.

EVs released apically from either control or H_2O_2-stimulated ARPE-19 cell monolayers or unstimulated J- or H-cybrid monolayers were isolated and equal numbers were transferred to stimulate naïve ARPE-19 cell monolayers. TER measurements between time point 0 (baseline) and 4 h (post treatment) were obtained. EVs collected from stressed ARPE-19 cells (exposed to 0.5 mM H_2O_2; "stress EVs") elicited a drop in TER (bystander effect) in naive recipient cells ($P < 0.0001$), whereas EVs released from control cells ("control EVs") had no effect on TER by the four-hour time point (Fig. 2A), confirming our previous results [20]. Interestingly, EVs released from H-cybrids behaved like exosomes released from control ARPE-19 cells, whereas J-cybrids elicited a reduction in TER similar in magnitude as that of stress EVs ($P < 0.0001$).

We have explored the mechanism of action of EVs in TER reduction previously. Specifically we have shown that EVs are required to induce the effect, since the media from which the EVs were depleted failed to results in a drop in TER [20], as did the addition of the endocytosis inhibitor (dynasore) [20]. In addition, we have examined the role of ligands involved in EV uptake in two previous studies, examining stress EVs when compared to control EVs. Specifically, known ligand-receptor and lipid-based interactions were probed using specific inhibitors. Stress EV uptake was found not to be mediated by lipid raft-mediated internalization, as pretreatment with filipin, a known blocker of lipid interactions that prevents EV uptake in other cells [36], was found to be ineffective. On the flipside, ligand-receptor interactions were found to be critical, including immunoglobulin-integrin

interaction or integrin-matrix macromolecule interactions as well as proteogylcans and their modifications [2]. Specifically, interfering with integrin signaling using the RGD peptide which blocks the interaction between integrin and its ligands, pretreatment of recipient cells with heparinase to remove surface proteoglycans or removal of annexin A2 by siRNA knockdown prevented the drop in TER after exposure to stress EVs [20,27].

Similarly, the effects of J-cybrid EVs on TER of recipient ARPE-19 cells could not be prevented by filipin; both filipin-treated and untreated J-cybrid EVs resulted in a ~ 20% drop in TER after 4 h (Fig. 2B). However, pretreatment of the naive recipient cells with either RGD peptide or heparinase prevented the drop in TER after exposure to J-cybrid EVs (Fig. 2B). Taken together, a similar set of interactions based on protein- rather than lipid-based interactions appear to mediate the uptake of EVs from both oxidatively stressed (H_2O_2) and metabolically stressed (J-haplogroup) RPE cells.

3.2. Cybrid EV uptake analysis using live-cell imaging in ARPE-19 cells

EV internalization by RPE monolayers was analyzed using confocal microscopy [20]. The naïve recipient RPE cells were labeled with CellTracker (red) and Hoechst (blue) to visualize cytoplasm and nuclei, respectively; and EVs added to the cells were labeled with the RNA dye ExoGlow (green). Intracellular EVs can be identified based on the co-localization of cytoplasm (red) and RNA (green) on a per-dot basis. This technique had allowed us to demonstrate that stress EVs were rapidly taken up by naïve ARPE-19 cells, and their uptake could be inhibited by the same inhibitors that interfered with TER reduction, RGD peptide and heparinase, but not filipin [27]. Similar to the control and stress EVs (H_2O_2) reported previously [20,27], H-cybrid showed little uptake over the 2 h imaging period, whereas uptake of J-cybrids was rapid and complete (Fig. 3A, B). Hence, the imaging experiments confirmed the similarity in behavior between stress EVs characterized previously [27] and those isolated from J-cybrids characterized here.

3.3. Analysis of ligands in cybrid EVs

Based on the similarities in the functional assays between the stress EVs and the cybrid EVs, the same ligands, annexin-A2, fibronectin and glypican, which were significantly elevated on stress EVs [20,27] were investigated here. EVs from J- and H-cybrid cells were analyzed by Western blotting (annexin-A2 [Fig. 4A'], fibronectin [Fig. 4B′]) and ELISA (glypican 1) using equal numbers of EVs per sample. J-cybrids EVs contain significantly more annexin A2 and fibronectin than H-cybrid EVs (Fig. 4A, B), whereas glypican levels were similar (H-EVs: 0.76 ± 0.19 ng/mL versus J-EVs: 1.00 ± 0.26 ng/mL; $P = 0.14$). Thus, ligands known to be required for EV uptake and implicated in uptake by inhibitor assays were elevated in J-cybrid EVs.

3.4. EVs contain HDAC6 cargo to generate bystander effect if enabled to enter the cells

The results presented above demonstrated that EVs from stress ARPE-19 cells and J-cybrids share many similarities. Both exhibit high levels of ligands presumably on the EV surface, and uptake leads to the reduction in barrier function. Previously we have identified HDAC6 as a cargo in EVs that can be transferred to recipient cells [20], where it is presumed to reduce tight junction stability by deacetylation of tubulin [37]. HDAC6 activity levels were

elevated in stress EVs, HDAC6 activity levels could be elevated in recipient cells upon EV transfer, and reduction in TER in response to EV uptake could be prevented by HDAC6 inhibitors tubastatin A and TSA [20] added either to the EVs or the recipient cells.

Here, HDAC6 activity levels were determined using a homogenous fluorescence release HDAC deacetylase assay (Fig. 5A). Levels were found to be identical between EVs isolated from control ARPE-19 cell cultures, H- and J-cybrids; and levels were elevated in EVs isolated from H_2O_2-treated H-cybrid cells but not J-cybrid cells. To determine if inhibiting HDAC6 would prevent the drop in TER induced by J-cybrids, recipient cells were pretreated with TSA prior to addition of EVs (Fig. 5B). Pretreatment of the recipient cells with TSA alone had no effect on TER ([20] and data not shown), but in the presence of J-cybrid EVs prevented the drop in TER. These results further support our previous conclusion that the levels of HDAC6 present in control, J- and H-cybrids are sufficient to reduce TER when aided to enter the cells by the presence of ligands (fibronectin, annexin A2) involved in EV uptake. In addition, the effect of HDAC6 transfer by EVs is not specific to H_2O_2-treated ARPE-19 cells, but can be extended to other cells under stress conditions such as the J-cybrids with reduced metabolic capacity.

4. Discussion

The main results of the current study are: 1) In comparison to H-cybrids, J-cybrid cells develop monolayers with reduced barrier function, and ATP synthesis is reduced in both aerobic phosphorylation and glycolysis; 2) Addition of EVs released from J- but not H-cybrids to naïve RPE monolayers resulted in TER reduction, and EV uptake was confirmed by imaging; 3) Two ligand-receptor interactions, integrins and proteoglycans known to be involved in stress EV uptake by naïve RPE cells were demonstrated to also be necessary for J-cybrid EV uptake; 4) Elevated levels of fibronectin and annexin A2 were identified on J-cybrid EVs compared to H-cybrid EVs; and 5) HDAC6 signaling was identified as a mechanism involved in J-cybrid EV induced TER reduction. In summary, these results suggest that EVs from stressed RPE cells exhibit an overlapping profile of ligands irrespective of how stress is created, H_2O_2 exposure or mitochondrial energy crisis; and that this profile differs from those of control cells. It will be great importance to demonstrate whether these ligands can be used as a diagnostic of RPE health or dysfunction.

RPE alterations can be caused by environmental and/or genetic stressors. Only recently have we started to investigate the mitochondrial genome and its haplogroups as one of the potential genetic risk factors for disease. Mitochondria are a multi-functional organelle. They are responsible for energy metabolism using the TCA cycle, OXPHOS, and beta-oxidation of fatty acids as well as calcium homeostasis. These roles, together with their ability to produce reactive oxygen species (ROS), tie them into the control of cell survival and apoptosis. Mitochondria, which are passed down via the maternal lineage of inheritance, carry their own circular DNA with 16,569 nucleotide pairs, encoding 37 genes including 13 protein subunits required for OXPHOS. mtDNA, like nuclear DNA has accumulated specific SNPs to adapt to diseases and environments. The two haplogroups under investigation are both from Europe, with the H-haplogroup representing the most common European haplogroup, and the J-haplogroup representing an adaptation to the colder climate of

Northern Europe with SNP variants resulting in a less tightly coupled ECT chain and greater heat production [38]. Perhaps not surprisingly, certain haplogroups are associated with age-related macular degeneration (AMD), with the J-, T- and U-haplogroups representing high risk, the H-haplogroup representing low risk or even protection [8–12]. While it is still unclear how mtDNA haplogroups contribute to disease risk, the use of cytoplasmic hybrids has started to contribute to our understanding of how mtDNA SNP variants contribute to cellular behavior in the context of identical nuclear DNA. One of our laboratories (Kenney) has developed human ARPE-19 cell cybrids, by introducing mitochondria from individuals with H- or J-haplogroups [13]. In the original publication [13], it was confirmed that the two haplogroups have identical mtDNA copy number. It was reported that while H-cybrids have higher baseline ATP production, as a side product, they also generate higher levels of ROS than the J-cybrids. H-cybrids grow slower, and the two haplogroups differ in the expression of nuclear genes involved in inflammation and human retinal diseases. Here we expanded the analysis of cellular behavior into their ability to form monolayers and an extended analysis into energy metabolism. The slower growing H-cybrids were found to develop better barrier function than the faster growing J-cybrids, with TER values differing significantly by ~15%. A careful analysis of the cybrids' energy metabolism using Seahorse assays revealed partial agreement between our findings and that of the original Kenney lab publication, using different techniques [28]. OCR measurements confirmed that H-cells have higher levels of OXPHOS and glycolysis. H-cybrids when compared to J-cybrids exhibit higher basal respiration, ATP production and maximum respiration, with the coupling efficiency of the ECT being tighter, leading to a lower proton leak. The biggest difference between H- and J-cybrids was the reduced effect of shutting down complex V with oligomycin, suggesting impaired ATP synthase activity. ECAR measurements in response to oligomycin also suggest that the rate of glycolysis is significantly reduced in J- when compared to H-cybrids. Our results are identical to those generated in Seahorse assays of human osteosarcoma cell line 143B.TK- H- and J-cybrids, which document a reduced glycolytic rate and decreased OXPHOS in J- compared to H-cybrids [39]. In contrast, Kenney and coworkers report an increase in ATP production for RPE H-cybrids using a luminescence ATP detection assay, but lower levels of glycolysis based on an overall increase in lactate production [13]. One of the critical differences is the media in which measurements are made; here, our Seahorse assays use substrate conditions optimized for OXPHOS, whereas Kenney et al. plated the cybrids in DMEM-F12 + 10% FBS for 24 h, rinsed with Seahorse assay media and then conducted the assay using Seahorse based media comprised of DMEM supplemented with 17.5 mM glucose, 10 mM sodium pyruvate and 2 mM L-glutamine. Their use of 10% FBS immediately prior to the assay may provide excess substrate for a Warburg-like (aerobic glycolysis) metabolic profile. In addition is likely that the faster growing J-cybrids under growth promoting conditions (10% FBS promotes RPE cell growth, 1% promotes differentiation [30]) generate most of their energy needed for growth using aerobic glycolysis rather than OXPHOS [40]. Moreover, Kenney normalized the Seahorse data to total protein from each well while we normalized to area of wells covered by cells. Finally, plotting ECAR against OCR levels provides a snap-shot of the bioenergetics profiles of a particular cell, which demonstrates that H-cybrids exhibit a higher energy metabolism and increased capacity to respond to changes, when compared to J-cybrids (Fig. 1E). Based on the SNP analysis, which revealed that cells with

H-mitochondria carry a SNP in Cytochrome c oxidase, subunit 1 (complex IV), whereas those with J-mitochondria harbor a SNPs in NADH dehydrogenase, subunit 5 (complex I), there are two potential scenarios that could indirectly contribute to a reduction in complex V activity and ATP production: first, the SNP in complex IV might increase the proton gradient in H-cells and/or the SNP in NADH dehydrogenase could reduce the proton gradient in J-cells by reducing the amount of NADH as the electron donor for the ETC.

Based on the differences in energy metabolism it is expected that H-cybrids might represent a healthier, less metabolically stressed cells than J-cybrids. Here we tested whether the difference in mitochondrial function might be reflected in the profile of the EVs. EVs were isolated by ExoQuick, a polyethylene glycol-based precipitation method. While used widely due to its ease of use, it may also precipitate other components such as lipid droplets and other vesicular and non-vesicular entities. We have eliminated the presence of lipid droplets based on the lack of ApoB present in our preparations [20]. However, other protein contaminants cannot be excluded. A useful measure of purity of sample is the ratio of number of particles to protein concentration [41]. Based on the measured protein concentration of 1.54 ± 0.27 μg/mL, this corresponds to a ratio of number of EVs to protein concentration of $1.79 \pm 0.29 \times 10^{10}$, which based on Webber and Clayton [41] represents a value between low purity (ratios of 2×10^9 to 2×10^{10} particles/μg protein) and high purity ($>3 \times 10^{10}$ particles/μg protein). Therefore, while the results based on cargo (HDAC6) and EV ligands (annexin A2 and fibronectin) interacting with receptors on the recipient cells, speak in favor of vesicles being endocytosed, we cannot exclude that contaminants pulled down together with EVs may contribute to the observed effects. H- and J-cybrids when compared to their parent ARPE-19 cells (U5 haplogroup) release similar amounts of EVs to the apical side with a similar diameter; however, they differ in their ability to induce a bystander effect. The bystander effect refers to the observation that biological effects can be induced in cells that are not directly targeted, with the neighboring or naïve cells being affected by cell-cell communication via gap junctions, or long-distance via secreted material such as EVs [42]. In RPE cells, both ARPE-19 and primary pig RPE cells, we have shown that oxidatively stressed cells can communicate these stress messages to naïve healthy cells via EVs [20]. Our reported bystander effect triggered by the EVs results in a reduction in barrier function in naïve RPE monolayers. It is dependent on ligand-mediated endocytosis [20,27], and one of the cargo molecules mediating the effect is HDAC6 [20]. The ligand included fibronectin and annexin A2, mediating integrin and heparin sulfate proteoglycan-mediated EV uptake. Here we showed that EVs from J-cybrids elicited the bystander effect in an HDAC6 dependent manner, and uptake could be inhibited by interfering with integrin signaling or by removing heparin sulfate proteoglycans. Finally, and maybe most importantly, EVs from J-cybrids contained significantly elevated levels of fibronectin and annexin A2. Hence this is the third preparation, H_2O_2-stressed ARPE-19 cells, H_2O_2-stressed primary pig RPE cells, and now J-cybrids that exhibit this signature. Fibronectin and annexin-A2 were also identified in primary pig RPE EVs by the Bowes-Rickman lab using mass-spectrometry [43]. Other than higher levels of annexin A2 in stress RPE EVs, annexin A2 in EVs has been shown to represent a marker for breast cancer metastasis and promote angiogenesis [44], and annexin A2 has been show to play a role in attachment and entry of multiple epithelial cell-targeting viruses – with virus uptake sharing

many similarities with EV uptake [45]. How does annexin A2 partition into EVs under oxidative stress? In general, annexin A2 is a membrane curvature-inducing protein that can contribute to the formation of vesicles [46], and has been suggested to be involved in endocytic and exocytic vesicular transport. Interestingly, annexin A2 has been identified as a novel cellular redox regulatory protein [47]. Specifically, the group showed that annexin A2 possesses an N-terminal reactive cysteine residue that can be oxidized by H_2O_2, followed by reduction by the thioredoxin system. This reversible oxidation allows annexin A2 to participate in multiple redox cycles. Thus, it is plausible that after multiple redox cycles, oxidized annexin A2 is packaged into EVs for removal from the cells. Fibronectin, like annexin, has been shown to be elevated on circulating EVs of breast cancer patients [48], myeloma cell-derived EVs [49] or fibroblasts isolated from human subjects with an age-related lung disorder [50]. While subcytotoxic oxidative stress with H_2O_2, has been shown to increase the steady-state level of fibronectin in fibroblasts [51] and RPE cells [52], fibronectin has also been suggested to also be a pro-survival component of EVs released from melanocytes in response to UV-B radiation [53] a stressor known to produce H_2O_2 [54]. For fibronectin and annexin A2 to be of use as biomarkers of the metabolic state of RPE cells, additional markers for the isolation or enrichment of RPE-derived EVs from biological fluids such as vitreous humor or serum need to be developed [55].

In conclusion, we further confirmed a receptor-mediated uptake mechanism that appears to be common for EVs released from stressed RPE cells by naïve RPE cells. In addition, we have confirmed that fibronectin and annexin A2 are present at elevated levels on EVs not only in EVs from H_2O_2-stressed, but also from metabolically stressed RPE cells. These findings will aid with the development of future biomarkers characterizing the health of the RPE.

Acknowledgements

In the Rohrer laboratory, the study was supported in part by the Department of Veterans Affairs (I01RX000444, I01BX003050 and IK6BX004858), the National Institutes of Health (R01EY024581), and the South Carolina SmartState Endowment; Cris Kenney is supported by NIH R01EY0127363 and Unrestricted grants to the Department of Ophthalmology from Research to Prevent Blindness, New York, NY and the Discovery Eye Foundation, Los Angeles, CA. The authors would like to thank James Chao for help with the HDAC6 assay.

References

[1]. Zarbin MA, Current concepts in the pathogenesis of age-related macular degeneration, Arch. Ophthalmol122 (2004) 598–614. [PubMed: 15078679]

[2]. Velilla S, Garcia-Medina JJ, Garcia-Layana A, Dolz-Marco R, Pons-Vazquez S, Pinazo-Duran MD, Gomez-Ulla F, Arevalo JF, Diaz-Llopis M, Gallego-Pinazo R, Smoking and age-related macular degeneration: review and update, J. Ophthalmol2013 (2013) 895147. [PubMed: 24368940]

[3]. Tan PL, Bowes Rickman C, Katsanis N, AMD and the alternative complement pathway: genetics and functional implications, Hum Genomics10 (2016) 23. [PubMed: 27329102]

[4]. Hageman GS, Luthert PJ, Victor Chong NH, Johnson LV, Anderson DH, Mullins RF, An integrated hypothesis that considers drusen as biomarkers of immune-mediated processes at the RPE-Bruch's membrane interface in aging and age-related macular degeneration, Prog. Retin. Eye Res20 (2001) 705–732. [PubMed: 11587915]

[5]. Kanow MA, Giarmarco MM, Jankowski CS, Tsantilas K, Engel AL, Du J, Linton JD, Farnsworth CC, Sloat SR, Rountree A, Sweet IR, Lindsay KJ, Parker ED, Brockerhoff SE, Sadilek M, Chao

JR, Hurley JB, Biochemical adaptations of the retina and retinal pigment epithelium support a metabolic ecosystem in the vertebrate eye, Elife6 (2017) e28899. [PubMed: 28901286]

[6]. Kenney MC, Chwa M, Atilano SR, Falatoonzadeh P, Ramirez C, Malik D, Tarek M, Del Carpio JC, Nesburn AB, Boyer DS, Kuppermann BD, Vawter MP, Jazwinski SM, Miceli MV, Wallace DC, Udar N, Molecular and bioenergetic differences between cells with African versus European inherited mitochondrial DNA haplogroups: implications for population susceptibility to diseases, Biochim. Biophys. Acta1842 (2014) 208–219. [PubMed: 24200652]

[7]. van Oven M, Kayser M, Updated comprehensive phylogenetic tree of global human mitochondrial DNA variation, Hum. Mutat30 (2009) E386–E394. [PubMed: 18853457]

[8]. Canter JA, Olson LM, Spencer K, Schnetz-Boutaud N, Anderson B, Hauser MA, Schmidt S, Postel EA, Agarwal A, Pericak-Vance MA, Sternberg P Jr., Haines JL, Mitochondrial DNA polymorphism A4917G is independently associated with age-related macular degeneration, PLoS One3 (2008), e2091. [PubMed: 18461138]

[9]. Jones MM, Manwaring N, Wang JJ, Rochtchina E, Mitchell P, Sue CM, Mitochondrial DNA haplogroups and age-related maculopathy, Arch. Ophthalmol125 (2007) 1235–1240. [PubMed: 17846364]

[10]. Udar N, Atilano SR, Memarzadeh M, Boyer DS, Chwa M, Lu S, Maguen B, Langberg J, Coskun P, Wallace DC, Nesburn AB, Khatibi N, Hertzog D, Le K, Hwang D, Kenney MC, Mitochondrial DNA haplogroups associated with age-related macular degeneration, Invest. Ophthalmol. Vis. Sci50 (2009) 2966–2974. [PubMed: 19151382]

[11]. SanGiovanni JP, Arking DE, Iyengar SK, Elashoff M, Clemons TE, Reed GF, Henning AK, Sivakumaran TA, Xu X, DeWan A, Agron E, Rochtchina E, Sue CM, Wang JJ, Mitchell P, Hoh J, Francis PJ, Klein ML, Chew EY, Chakravarti A, Mitochondrial DNA variants of respiratory complex I that uniquely characterize haplogroup T2 are associated with increased risk of age-related macular degeneration, PLoS One4 (2009), e5508. [PubMed: 19434233]

[12]. Mueller EE, Schaier E, Brunner SM, Eder W, Mayr JA, Egger SF, Nischler C, Oberkofler H, Reitsamer HA, Patsch W, Sperl W, Kofler B, Mitochondrial haplogroups and control region polymorphisms in age-related macular degeneration: a case-control study, PLoS One7 (2012), e30874. [PubMed: 22348027]

[13]. Kenney MC, Chwa M, Atilano SR, Pavlis JM, Falatoonzadeh P, Ramirez C, Malik D, Hsu T, Woo G, Soe K, Nesburn AB, Boyer DS, Kuppermann BD, Jazwinski SM, Miceli MV, Wallace DC, Udar N, Mitochondrial DNA variants mediate energy production and expression levels for CFH, C3 and EFEMP1 genes: implications for age-related macular degeneration, PLoS One8 (2013), e54339. [PubMed: 23365660]

[14]. Wilkins HM, Carl SM, Swerdlow RH, Cytoplasmic hybrid (cybrid) cell lines as a practical model for mitochondriopathies, Redox Biol2 (2014) 619–631. [PubMed: 25460729]

[15]. Rohrer B, Bandyopadhyay M, Beeson C, Reduced metabolic capacity in aged primary retinal pigment epithelium (RPE) is correlated with increased susceptibility to oxidative stress, Adv. Exp. Med. Biol854 (2016) 793–798. [PubMed: 26427491]

[16]. Karunadharma PP, Nordgaard CL, Olsen TW, Ferrington DA, Mitochondrial DNA damage as a potential mechanism for age-related macular degeneration, Invest. Ophthalmol. Vis. Sci51 (2010) 5470–5479. [PubMed: 20505194]

[17]. Ferrington DA, Kapphahn RJ, Leary MM, Atilano SR, Terluk MR, Karunadharma P, Chen GK, Ratnapriya R, Swaroop A, Montezuma SR, Kenney MC, Increased retinal mtDNA damage in the CFH variant associated with age-related macular degeneration, Exp. Eye Res145 (2016) 269–277. [PubMed: 26854823]

[18]. Ishii M, Rohrer B, Bystander effects elicited by single-cell photo-oxidative blue-light stimulation in retinal pigment epithelium cell networks, Cell Death Discov3 (2017) 16071. [PubMed: 28179989]

[19]. Ishii M, Rohrer B, Mechanisms of bystander effects in retinal pigment epithelium cell networks, Cell Death Dis8 (2017), e3061. [PubMed: 28981111]

[20]. Shah N, Ishii M, Brandon C, Ablonczy Z, Cai J, Liu Y, Chou CJ, Rohrer B, Extracellular vesicle-mediated long-range communication in stressed retinal pigment epithelial cell monolayers, Biochim. Biophys. Acta1864 (2018) 2610–2622.

[21]. Bayraktar E, Abd-Ellah MF, Amero P, Chavez-Reyes A, Rodriguez-Aguayo C, Exosomes: from garbage bins to promising therapeutic targets, Int. J. Mol. Sci18 (2017).

[22]. Antwi-Baffour SS, Molecular characterisation of plasma membrane-derived vesicles, J. Biomed. Sci22 (2015) 68. [PubMed: 26259622]

[23]. Thery C, Witwer KW, Aikawa E, Alcaraz MJ, Anderson JD, Andriantsitohaina R, Antoniou A, Arab T, Archer F, Atkin-Smith GK, Ayre DC, Bach JM, Bachurski D, Baharvand H, Balaj L, Baldacchino S, Bauer NN, Baxter AA, Bebawy M, Beckham C, Bedina Zavec A, Benmoussa A, Berardi AC, Bergese P, Bielska E, Blenkiron C, Bobis-Wozowicz S, Boilard E, Boireau W, Bongiovanni A, Borras FE, Bosch S, Boulanger CM, Breakefield X, Breglio AM, Brennan MA, Brigstock DR, Brisson A, Broekman ML, Bromberg JF, Bryl-Gorecka P, Buch S, Buck AH, Burger D, Busatto S, Buschmann D, Bussolati B, Buzas EI, Byrd JB, Camussi G, Carter DR, Caruso S, Chamley LW, Chang YT, Chen C, Chen S, Cheng L, Chin AR, Clayton A, Clerici SP, Cocks A, Cocucci E, Coffey RJ, Cordeiro-da-Silva A, Couch Y, Coumans FA, Coyle B, Crescitelli R, Criado MF, D'Souza-Schorey C, Das S, Datta Chaudhuri A, de Candia P, De Santana EF, De Wever O, Del Portillo HA, Demaret T, Deville S, Devitt A, Dhondt B, Di Vizio D, Dieterich LC, Dolo V, Dominguez Rubio AP, Dominici M, Dourado MR, Driedonks TA, Duarte FV, Duncan HM, Eichenberger RM, Ekstrom K, El Andaloussi S, Elie-Caille C, Erdbrugger U, Falcon-Perez JM, Fatima F, Fish JE, Flores-Bellver M, Forsonits A, Frelet-Barrand A, Fricke F, Fuhrmann G, Gabrielsson S, Gamez-Valero A, Gardiner C, Gartner K, Gaudin R, Gho YS, Giebel B, Gilbert C, Gimona M, Giusti I, Goberdhan DC, Gorgens A, Gorski SM, Greening DW, Gross JC, Gualerzi A, Gupta GN, Gustafson D, Handberg A, Haraszti RA, Harrison P, Hegyesi H, Hendrix A, Hill AF, Hochberg FH, Hoffmann KF, Holder B, Holthofer H, Hosseinkhani B, Hu G, Huang Y, Huber V, Hunt S, Ibrahim AG, Ikezu T, Inal JM, Isin M, Ivanova A, Jackson HK, Jacobsen S, Jay SM, Jayachandran M, Jenster G, Jiang L, Johnson SM, Jones JC, Jong A, Jovanovic-Talisman T, Jung S, Kalluri R, Kano SI, Kaur S, Kawamura Y, Keller ET, Khamari D, Khomyakova E, Khvorova A, Kierulf P, Kim KP, Kislinger T, Klingeborn M, Klinke DJ, Kornek M, Kosanovic MM, Kovacs AF, Kramer-Albers EM, Krasemann S, Krause M, Kurochkin IV, Kusuma GD, Kuypers S, Laitinen S, Langevin SM, Languino LR, Lannigan J, Lasser C, Laurent LC, Lavieu G, Lazaro-Ibanez E, Le Lay S, Lee MS, Lee YXF, Lemos DS, Lenassi M, Leszczynska A, Li IT, Liao K, Libregts SF, Ligeti E, Lim R, Lim SK, Line A, Linnemannstons K, Llorente A, Lombard CA, Lorenowicz MJ, Lorincz AM, Lotvall J, Lovett J, Lowry MC, Loyer X, Lu Q, Lukomska B, Lunavat TR, Maas SL, Malhi H, Marcilla A, Mariani J, Mariscal J, Martens-Uzunova ES, Martin-Jaular L, Martinez MC, Martins VR, Mathieu M, Mathivanan S, Maugeri M, McGinnis LK, McVey MJ, Meckes DG Jr., Meehan KL, Mertens I, Minciacchi VR, Moller A, Jorgensen M. Moller, Morales-Kastresana A, Morhayim J, Mullier F, Muraca M, Musante L, Mussack V, Muth DC, Myburgh KH, Najrana T, Nawaz M, Nazarenko I, Nejsum P, Neri C, Neri T, Nieuwland R, Nimrichter L, Nolan JP, Nolte Hoen EN, Hooten N. Noren, O'Driscoll L, O'Grady T, O'Loghlen A, Ochiya T, Olivier M, Ortiz A, Ortiz LA, Osteikoetxea X, Ostergaard O, Ostrowski M, Park J, Pegtel DM, Peinado H, Perut F, Pfaffl MW, Phinney DG, Pieters BC, Pink RC, Poon IK, Powell BH, Prada I, Pulliam L, Quesenberry P, Radeghieri A, Raffai RL, Raimondo S, Rak J, Ramirez MI, Raposo G, Rayyan MS, Regev-Rudzki N, Ricklefs FL, Robbins PD, Roberts DD, Rodrigues SC, Rohde E, Rome S, Rouschop KM, Rughetti A, Russell AE, Saa P, Sahoo S, Salas-Huenuleo E, Sanchez C, Saugstad JA, Saul MJ, Schiffelers RM, Schneider R, Schoyen TH, Scott A, Shahaj E, Sharma S, Shatnyeva O, Shekari F, Shelke GV, Shetty AK, Shiba K, Siljander PR, Silva AM, Sodar BW, Soekmadji C, Sotillo J, Stahl PD, Stoorvogel W, Stott SL, Strasser EF, Swift S, Tahara H, Tewari M, Timms K, Tiwari S, Tixeira R, Tkach M, Toh WS, Tomasini R, Torrecilhas AC, Tosar JP, Toxavidis V, Urbanelli L, Vechetti IJ Jr., Veit TD, Vella LJ, Velot E, Verweij FJ, Vestad B, Vinas JL, Visnovitz T, Vukman KV, Wahlgren J, Watson DC, Wauben MH, Weaver A, Webber JP, Weber V, Wehman AM, Weiss DJ, Welsh JA, Wendt S, Wheelock AM, Wiener Z, Witte L, Wolfram J, Xagorari A, Xander P, Xu J, Yan X, Yanez-Mo M, Yin H, Yuana Y, Zappulli V, Zarubova J, Zekas V, Zhang JY, Zhao Z, Zheng L, Zheutlin AR, Zickler AM, Zimmermann P, Zivkovic AM, Zocco D, Zuba-Surma EK, Minimal information for studies of extracellular vesicles 2018 (MISEV2018): a position statement of the International Society for Extracellular Vesicles and update of the MISEV2014 guidelines, J. Extracell. Vesicles7 (2018) 1535750. [PubMed: 30637094]

[24]. Knickelbein JE, Liu B, Arakelyan A, Zicari S, Hannes S, Chen P, Li Z, Grivel JC, Chaigne-Delalande B, Sen HN, Margolis L, Nussenblatt RB, Modulation of immune responses by

extracellular vesicles from retinal pigment epithelium, Invest. Ophthalmol. Vis. Sci57 (2016) 4101–4107. [PubMed: 27537259]

[25]. Imjeti NS, Menck K, Egea-Jimenez AL, Lecointre C, Lembo F, Bouguenina H, Badache A, Ghossoub R, David G, Roche S, Zimmermann P, Syntenin mediates SRC function in exosomal cell-to-cell communication, Proc. Natl. Acad. Sci. U. S. A114 (2017) 12495–12500. [PubMed: 29109268]

[26]. Rajapakse D, Peterson K, Mishra S, Wistow G, Serum starvation of ARPE-19 changes the cellular distribution of cholesterol and Fibulin3 in patterns reminiscent of age-related macular degeneration, Exp. Cell Res361 (2017) 333–341. [PubMed: 29097185]

[27]. Nicholson C, Shah N, Ishii M, Annamalai B, Brandon C, Rodgers J, Nowling T, Rohrer B, Mechanisms of extracellular vesicle uptake in stressed retinal pigment epithelial cell monolayers, Biochim. Biophys. Acta Mol. Basis Dis2020 (1866) 165608.

[28]. Malik D, Hsu T, Falatoonzadeh P, Caceres-del-Carpio J, Tarek M, Chwa M, Atilano SR, Ramirez C, Nesburn AB, Boyer DS, Kuppermann BD, Jazwinski SM, Miceli MV, Wallace DC, Udar N, Kenney MC, Human retinal transmitochondrial cybrids with J or H mtDNA haplogroups respond differently to ultraviolet radiation: implications for retinal diseases, PLoS One9 (2014), e99003. [PubMed: 24919117]

[29]. Thurman JM, Renner B, Kunchithapautham K, Ferreira VP, Pangburn MK, Ablonczy Z, Tomlinson S, Holers VM, Rohrer B, Oxidative stress renders retinal pigment epithelial cells susceptible to complement-mediated injury, J. Biol. Chem284 (2009) 16939–16947. [PubMed: 19386604]

[30]. Ablonczy Z, Crosson CE, VEGF modulation of retinal pigment epithelium resistance, Exp. Eye Res85 (2007) 762–771. [PubMed: 17915218]

[31]. Perron NR, Beeson C, Rohrer B, Early alterations in mitochondrial reserve capacity; a means to predict subsequent photoreceptor cell death, J. Bioenerg. Biomembr45 (2013) 101–109. [PubMed: 23090843]

[32]. Consortium E-T, Van Deun J, Mestdagh P, Agostinis P, Akay O, Anand S, Anckaert J, Martinez ZA, Baetens T, Beghein E, Bertier L, Berx G, Boere J, Boukouris S, Bremer M, Buschmann D, Byrd JB, Casert C, Cheng L, Cmoch A, Daveloose D, De Smedt E, Demirsoy S, Depoorter V, Dhondt B, Driedonks TA, Dudek A, Elsharawy A, Floris I, Foers AD, Gartner K, Garg AD, Geeurickx E, Gettemans J, Ghazavi F, Giebel B, Kormelink TG, Hancock G, Helsmoortel H, Hill AF, Hyenne V, Kalra H, Kim D, Kowal J, Kraemer S, Leidinger P, Leonelli C, Liang Y, Lippens L, Liu S, Lo Cicero A, Martin S, Mathivanan S, Mathiyalagan P, Matusek T, Milani G, Monguio-Tortajada M, Mus LM, Muth DC, Nemeth A, O'Driscoll L, Palmulli R, Pfaffl MW, Primdal-Bengtson B, Romano E, Rousseau Q, Sahoo S, Sampaio N, Samuel M, Scicluna B, Soen B, Steels A, Swinnen JV, Takatalo M, Thaminy S, Thery C, Tulkens J, Van Audenhove I, van der Grein S, Van Goethem A, van Herwijnen MJ, Van Niel G, Van Roy N, Van Vliet AR, Vandamme N, Vanhauwaert S, Vergauwen G, Verweij F, Wallaert A, Wauben M, Witwer KW, Zonneveld MI, De Wever O, Vandesompele J, Hendrix A, EV-TRACK: transparent reporting and centralizing knowledge in extracellular vesicle research, Nat. Methods14 (2017) 228–232. [PubMed: 28245209]

[33]. Chou DH, Holson EB, Wagner FF, Tang AJ, Maglathlin RL, Lewis TA, Schreiber SL, Wagner BK, Inhibition of histone deacetylase 3 protects beta cells from cytokine-induced apoptosis, Chem. Biol19 (2012) 669–673. [PubMed: 22726680]

[34]. Soragni E, Chou CJ, Rusche JR, Gottesfeld JM, Mechanism of action of 2-Aminobenzamide HDAC inhibitors in reversing gene silencing in Friedreich's Ataxia, Front. Neurol6 (2015) 44. [PubMed: 25798128]

[35]. Tang Y-T, Huang Y-Y, Zheng L, Qin S-H, Xu X-P, An T-X, Xu Y, Wu Y-S, Hu X-M, Ping B-H, Wang Q, Comparison of isolation methods of exosomes and exosomal RNA from cell culture medium and serum, Int. J. Mol. Med40 (2017) 834–844. [PubMed: 28737826]

[36]. Mulcahy LA, Pink RC, Carter DR, Routes and mechanisms of extracellular vesicle uptake, J. Extracell. Vesicles 3 (2014).

[37]. Yano T, Matsui T, Tamura A, Uji M, Tsukita S, The association of microtubules with tight junctions is promoted by cingulin phosphorylation by AMPK, J. Cell Biol203 (2013) 605–614. [PubMed: 24385485]

[38]. Wallace DC, A mitochondrial paradigm of metabolic and degenerative diseases, aging, and cancer: a dawn for evolutionary medicine, Annu. Rev. Genet39 (2005) 359–407. [PubMed: 16285865]

[39]. Fernandez-Moreno M, Soto-Hermida A, Vazquez-Mosquera ME, Cortes-Pereira E, Relano S, Hermida-Gomez T, Pertega S, Oreiro-Villar N, Fernandez-Lopez C, Garesse R, Blanco FJ, Rego-Perez I, Mitochondrial DNA haplogroups influence the risk of incident knee osteoarthritis in OAI and CHECK cohorts. A meta-analysis and functional study, Ann. Rheum. Dis76 (2017) 1114–1122. [PubMed: 27919866]

[40]. Vander Heiden MG, Cantley LC, Thompson CB, Understanding the Warburg effect: the metabolic requirements of cell proliferation, Science324 (2009) 1029–1033. [PubMed: 19460998]

[41]. Webber J, Clayton A, How pure are your vesicles?J. Extracell. Vesicles2 (2013).

[42]. Hall EJ, The bystander effect, Health Phys85 (2003) 31–35. [PubMed: 12852468]

[43]. Klingeborn M, Dismuke WM, Skiba NP, Kelly U, Stamer WD, Bowes Rickman C, Directional exosome proteomes reflect polarity-specific functions in retinal pigmented epithelium monolayers, Sci. Rep7 (2017) 4901. [PubMed: 28687758]

[44]. Maji S, Chaudhary P, Akopova I, Nguyen PM, Hare RJ, Gryczynski I, Vishwanatha JK, Exosomal Annexin II promotes angiogenesis and breast Cancer metastasis, Mol. Cancer Res15 (2017) 93–105. [PubMed: 27760843]

[45]. Taylor JR, Skeate JG, Kast WM, Annexin A2 in virus infection, Front. Microbiol9 (2018) 2954. [PubMed: 30568638]

[46]. Morozova K, Sridhar S, Zolla V, Clement CC, Scharf B, Verzani Z, Diaz A, Larocca JN, Hajjar KA, Cuervo AM, Santambrogio L, Annexin A2 promotes phagophore assembly by enhancing Atg16L(+) vesicle biogenesis and homotypic fusion, Nat. Commun6 (2015) 5856. [PubMed: 25597631]

[47]. Madureira PA, Waisman DM, Annexin A2: the importance of being redox sensitive, Int. J. Mol. Sci14 (2013) 3568–3594. [PubMed: 23434659]

[48]. Moon PG, Lee JE, Cho YE, Lee SJ, Chae YS, Jung JH, Kim IS, Park HY, Baek MC, Fibronectin on circulating extracellular vesicles as a liquid biopsy to detect breast cancer, Oncotarget7 (2016) 40189–40199. [PubMed: 27250024]

[49]. Purushothaman A, Bandari SK, Liu J, Mobley JA, Brown EE, Sanderson RD, Fibronectin on the surface of myeloma cell-derived exosomes mediates exosome-cell interactions, J. Biol. Chem291 (2016) 1652–1663. [PubMed: 26601950]

[50]. Chanda D, Otoupalova E, Hough KP, Locy ML, Bernard K, Deshane JS, Sanderson RD, Mobley JA, Thannickal VJ, Fibronectin on the surface of extracellular vesicles mediates fibroblast invasion, Am. J. Respir. Cell Mol. Biol60 (2019) 279–288. [PubMed: 30321056]

[51]. Frippiat C, Chen QM, Zdanov S, Magalhaes JP, Remacle J, Toussaint O, Subcytotoxic H2O2 stress triggers a release of transforming growth factor-beta 1, which induces biomarkers of cellular senescence of human diploid fibroblasts, J. Biol. Chem276 (2001) 2531–2537. [PubMed: 11060295]

[52]. Yu AL, Fuchshofer R, Kook D, Kampik A, Bloemendal H, Welge-Lussen U, Subtoxic oxidative stress induces senescence in retinal pigment epithelial cells via TGF-beta release, Invest. Ophthalmol. Vis. Sci50 (2009) 926–935. [PubMed: 19171648]

[53]. Bin BH, Kim DK, Kim NH, Choi EJ, Bhin J, Kim ST, Gho YS, Lee AY, Lee TR, Cho EG, Fibronectin-containing extracellular vesicles protect melanocytes against ultraviolet radiation-induced cytotoxicity, J. Invest. Dermatol136 (2016) 957–966. [PubMed: 26854492]

[54]. Bertling CJ, Lin F, Girotti AW, Role of hydrogen peroxide in the cytotoxic effects of UVA/B radiation on mammalian cells, Photochem. Photobiol64 (1996) 137–142.

[55]. Klingeborn M, Skiba NP, Stamer WD, Bowes Rickman C, Isolation of retinal exosome biomarkers from blood by targeted Immunocapture, Adv. Exp. Med. Biol1185 (2019) 21–25. [PubMed: 31884583]

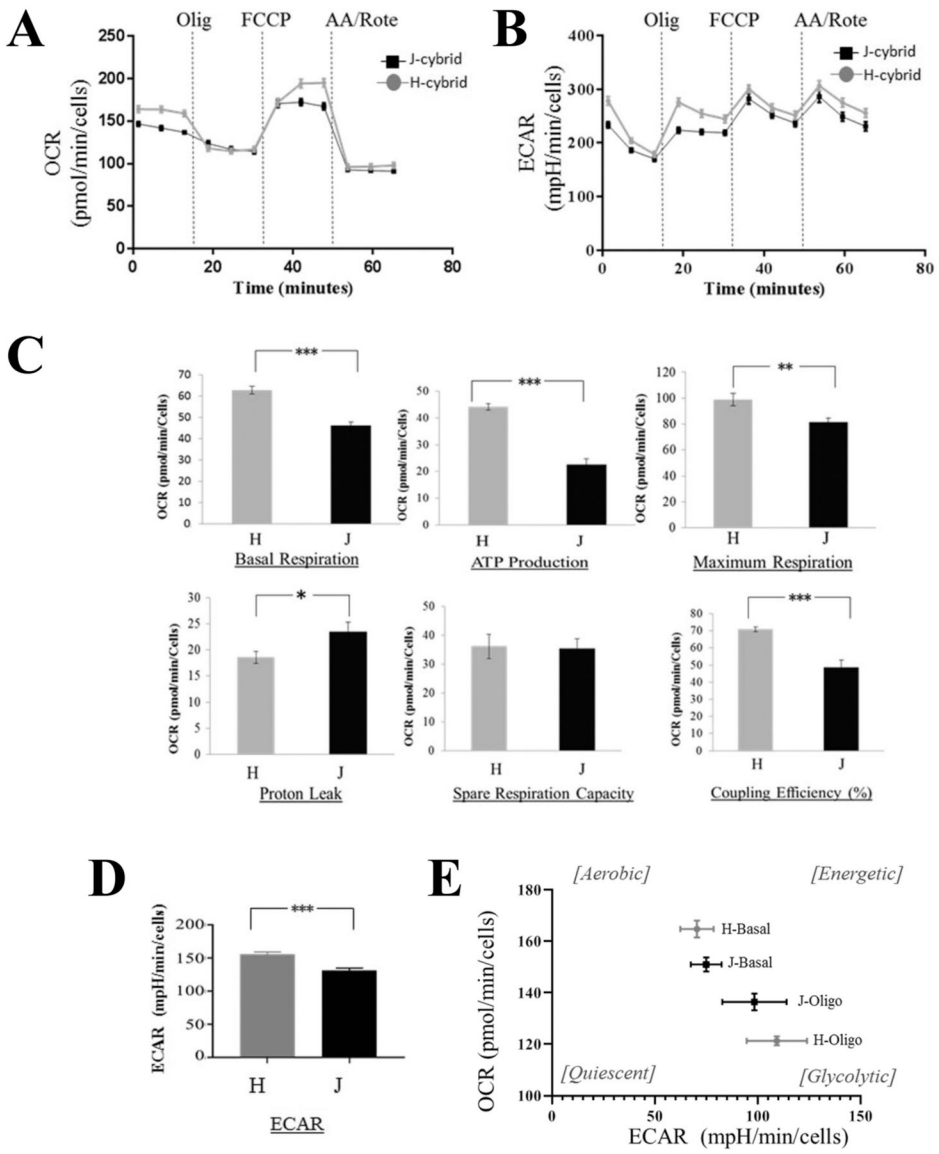

Fig. 1. Reduced energy metabolism in J-cybrids.

XFe96 high resolution respiratory assays were utilized on cybrids grown under serum starvation conditions, which promotes OXPHOS. (**A**) Basal respiration is measured in the presence of non-saturating substrate concentrations (5.6 mM glucose). The addition of oligomycin (inhibits ATP synthesis) reveals ATP production, the uncoupler FCCP (collapses the proton gradient across the mitochondrial inner membrane) reveals the maximum respiration and the spare respiratory capacity, the addition of antimycin A and rotenone (inhibitors of complex III and I) block all mitochondrial function to allow for the determination of non-mitochondrial respiration and proton leak. (**B**) Averaged traces of ECAR changes in response to oligomycin, FCCP and antimycin A + rotenone. (**C**) With the exception of spare respiratory capacity, all other features are impaired in J-cybrids. (**D**) Average ECAR levels changes in response to oligomycin are calculated. (**E**) OCR and ECAR levels normalized to values measured after antimycin A and rotenone injection

were plotted. H-cybrid metabolism at baseline is shifted towards a more aerobic state when compared to J-cybrids, and exhibit a greater dynamic range upon oligomycin treatment. Data is expressed as mean ± stdev, $n = 28/29$ independent replicates. Student's t-test *$P < 0.05$, ** $P < 0.01$, *** $P < 0.001$.

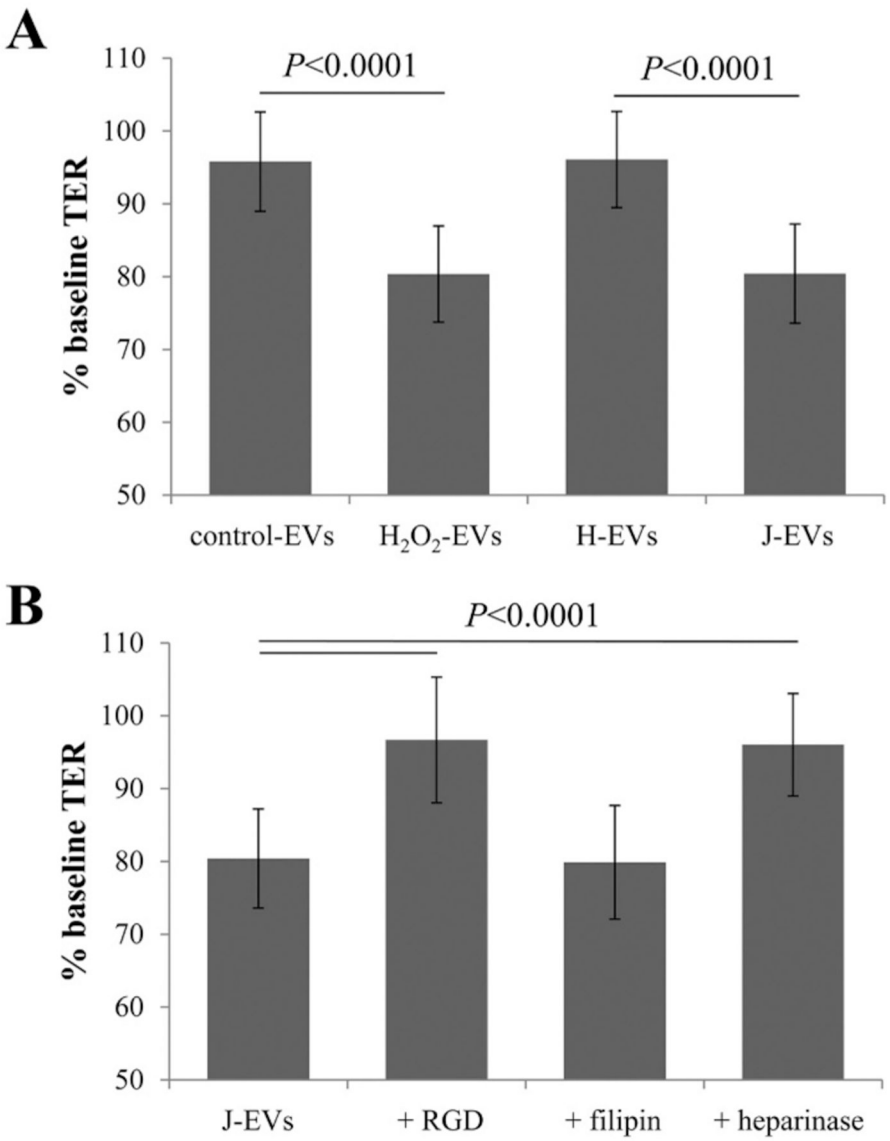

Fig. 2. Transfer assays to study cell-cell communication by EVs.

Transepithelial resistance (TER) assays are used to study bystander effects elicited by EV transfer as published, comparing TER measurements between 0 (baseline) and 4 h time point (post treatment). A reduction in TER is understood as successful uptake of EVs by recipient cells [20]. (**A**) EVs from ARPE-19 cell monolayers (donor cells) of control or stressed (H_2O_2) were transferred directly to the apical side of naïve monolayers (recipient cells). EVs from stressed cells reduced TER as reported [20]. EVs from H-cybrids (H EVs) behaved like control EVs, whereas J-cybrids (J EVs) behaved like H_2O_2 EVs. (**B**) Pretreatment of recipient cells with RGD peptide (integrin receptor inhibitor) or heparinase (removes surface proteoglycans) prevented TER reduction induced by J EVs, whereas pretreatment of EVs with filipin (inhibits lipid-based interaction) did not. Bar graphs represent mean ± stdev (n = 30–35). Significance was obtained using a posthoc ANOVA with Bonferroni correction.

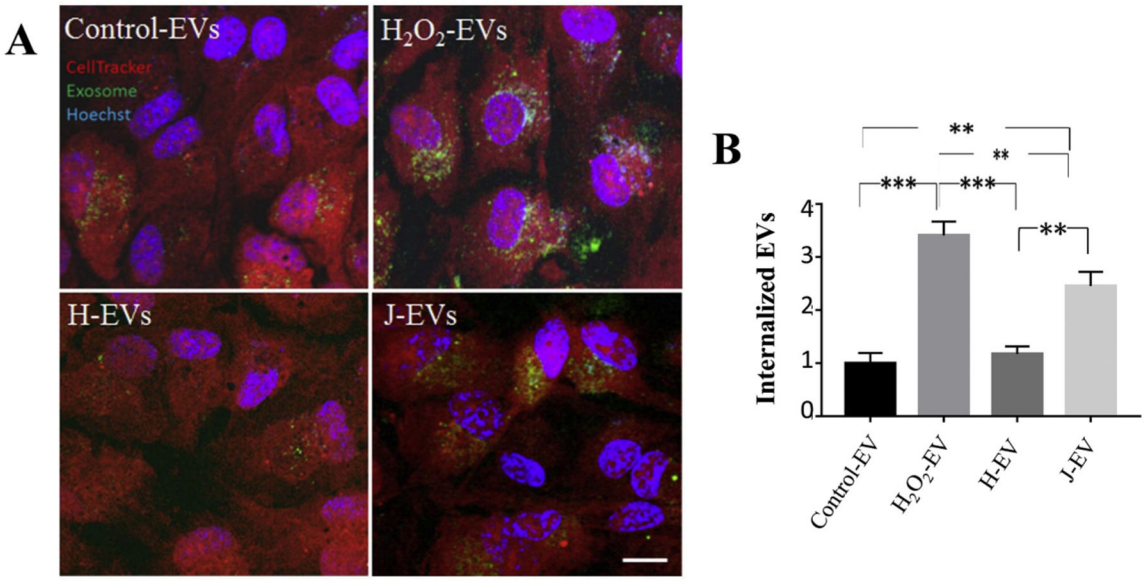

Fig. 3. Live cell imaging investigating ligand-dependent internalization of EVs.

(A) Images of live ARPE-19 cell monolayers exposed to EVs. EVs were labeled with ExoGlow (green), the cytoplasms of recipient cells were labeled with cell tracker (red) and nuclei with Hoechst (blue). Internalization of EVs was imaged by confocal; microscopy 120 min after the addition of EVs. Intracellular EVs were identified as co-localized dots between the red and green channel (= yellow). The yellow channel was binarized (representative examples in insets) and quantified in Image J. (**B**) Rapid uptake of J EVs in naïve ARPE-19 cells was confirmed but not H EVs. Graphs represent mean ± stdev (n = 4–8 wells, 6 locations each). Significance was obtained using a Student's t-test, ** $P < 0.001$, *** $P < 0.0001$.

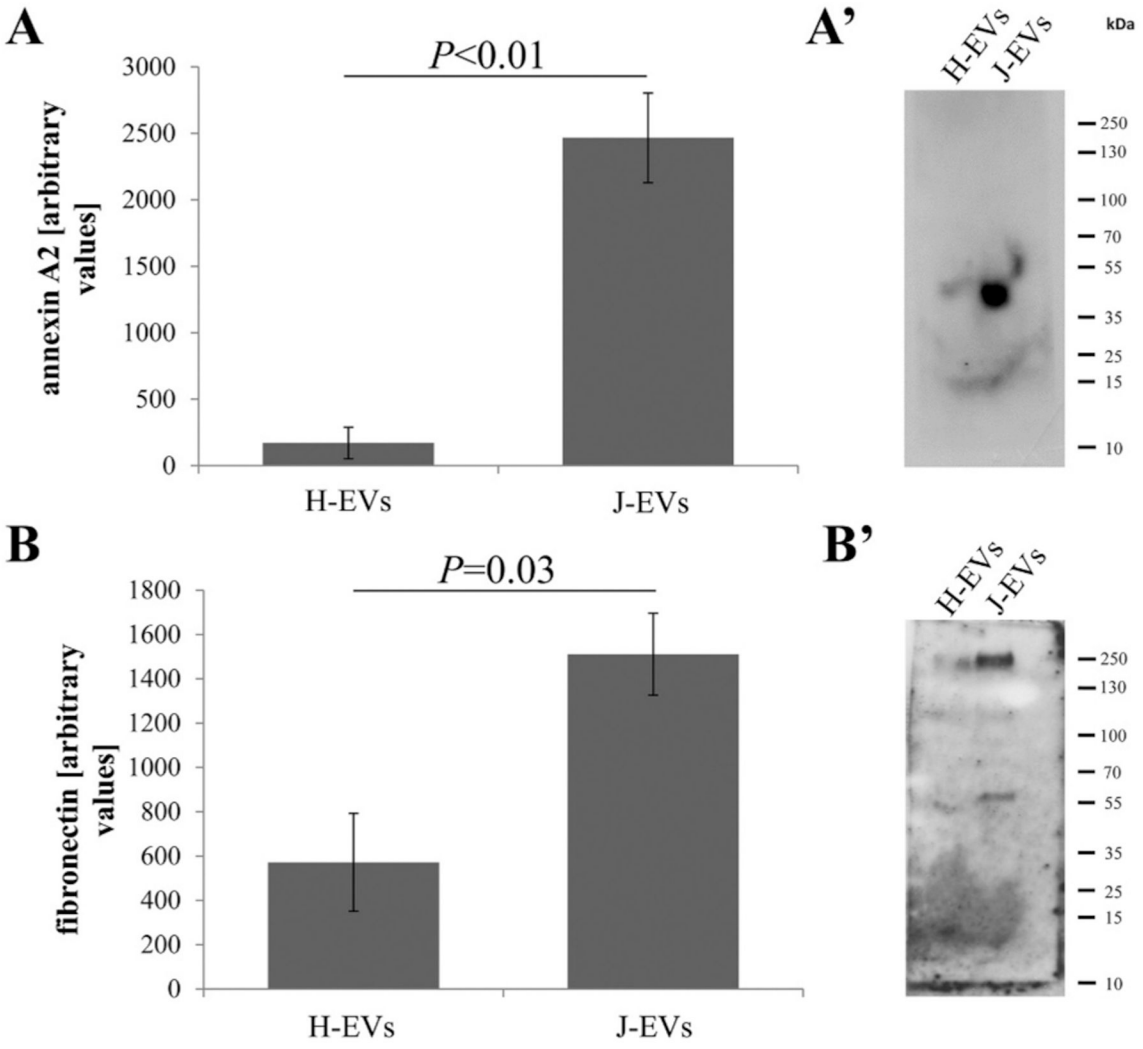

Fig. 4. EVs contain ligands required for uptake by recipient cells.

(A, A') Annexin-A2 (40 kDa) and (**B, B'**) fibronectin (220 kDa) levels were obtained by Western blotting, loading equal numbers of exosomes per sample. Both proteins were significantly elevated in EVs isolated from J-cybrids when compared to H-cybrids. Bar graphs represent mean ± SEM (n = 3 independent experiments). Significance was obtained using a t-test (Western, ELISA).

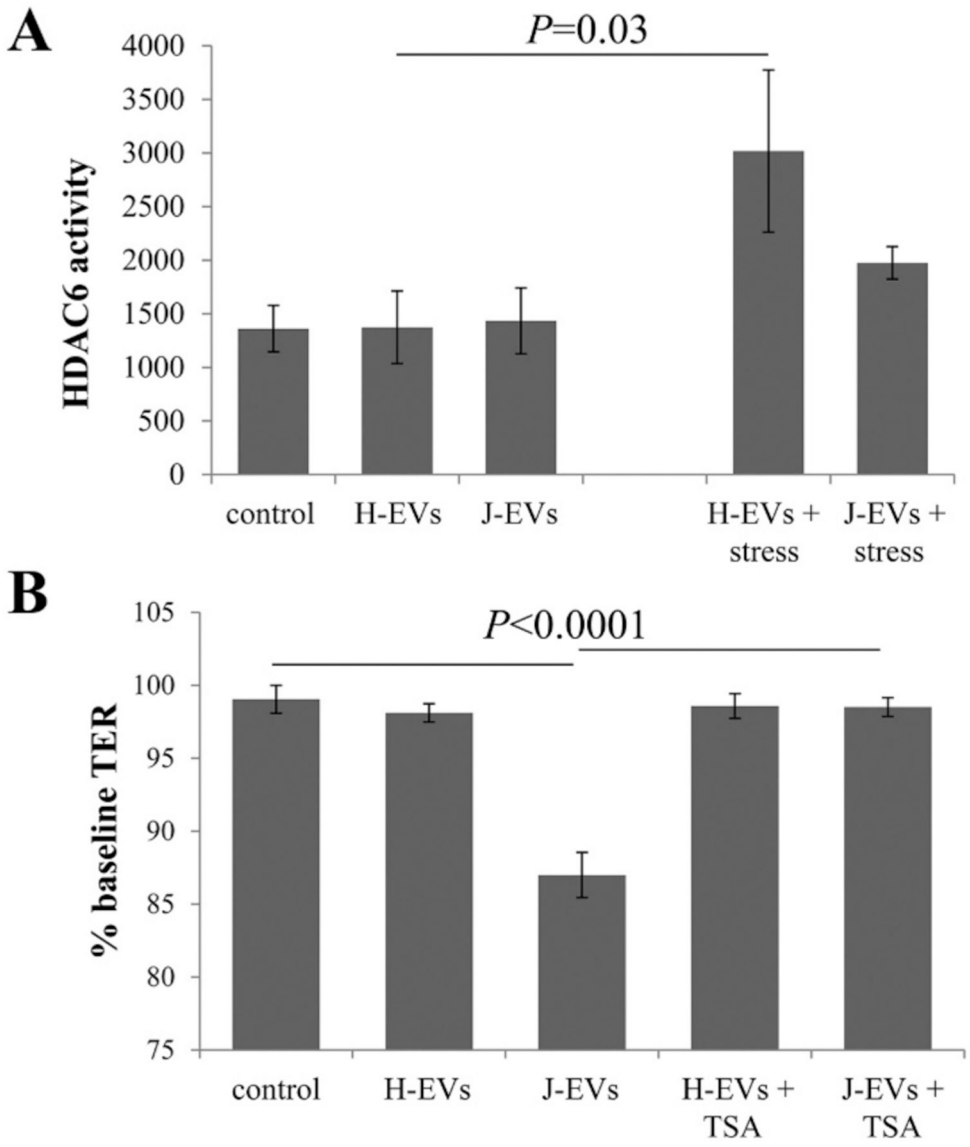

Fig. 5. Exosomes contain active HDAC6.

(A) HDAC activity was measured with a homogenous fluorescence release HDAC deacetylase assay in the presence of MS-275. HDAC6 activity was present at equal levels in EVs isolated from the apical compartment of ARPE-19 cells, J- and H-cybrids. Interestingly, HDAC6 levels could only be increased significantly in EVs from H- by not J-cybrids. Bar graph represent mean ± SEM, $n = 2–3$. (**B**) Transepithelial resistance (TER) assays were used to study bystander effects elicited by EV transfer as described in Figure Legend 3. Loss of TER in recipient cells in response to the transfer of EVs from J-cybrids is prevented by pre-treatment of recipient cells with HDAC6 inhibitor TSA. Bar graph represent mean ± SEM, $n = 9$. Significance was obtained using a posthoc ANOVA with Bonferroni correction.